Experimental study of stainless steel angles and channels in bending

Theofanous, Marios; Liew, Andrew; Gardner, Leroy

DOI:
10.1016/j.istruc.2015.10.004

Document Version
Peer reviewed version

Citation for published version (Harvard):
Theofanous, M, Liew, A & Gardner, L 2015, 'Experimental study of stainless steel angles and channels in bending', *Structures*, vol. 4, pp. 80-90. https://doi.org/10.1016/j.istruc.2015.10.004

Testing of stainless steel angles and channels in bending

M. Theofanous[a], A. Liew[b] and L. Gardner[c]

Please find attached our revised paper to be considered for publication in Structures, in the Euromech special issue.

[a] Lecturer, School of Civil Engineering, University of Birmingham, Birmingham B15 2TT, UK

Email: m.theofanous@bham.ac.uk

[b] Postdoctoral research associate, Institute of Structural Engineering, Swiss Federal Institute of Technology (ETH), Zurich, Switzerland.

[c] Professor of Structural Engineering, Department of Civil and Environmental Engineering, Imperial College London, London SW7 2AZ, UK

Email: leroy.gardner@imperial.ac.uk

Experimental study of stainless steel angles and channels in bending

M. Theofanous[a], A. Liew[b] and L. Gardner[c]

[a] Lecturer in Structural Engineering, School of Civil Engineering, University of Birmingham, Birmingham B15 2TT, UK. Email: m.theofanous@bham.ac.uk

[b] Postdoctoral Research Associate, Institute of Structural Engineering, Swiss Federal Institute of Technology (ETH), Zurich, Switzerland.

[c] Professor of Structural Engineering, Department of Civil and Environmental Engineering, Imperial College London, SW7 2AZ, UK. Email: leroy.gardner@imperial.ac.uk

Abstract

Substantial research has been conducted in recent years into the structural response of stainless steel components, with the focus being primarily on doubly symmetric cross-sections. Limited experimental data exist on non-doubly symmetric stainless steel sections in compression, while there is an absence of such data in bending, despite these sections being widely used in the construction industry as wind posts, lintels and so on. To address this limitation, and to bring an improved understanding of the behaviour of these sections, an experimental study into the flexural response of stainless steel channels bent about their minor axis and angles bent about their stronger geometric axis is described herein. In total, 16 bending tests on austenitic stainless steel beams have been conducted and the obtained results, including the full load-deformation history and observed failure modes have been described. Auxiliary tests on tensile coupons extracted from the tested sections and initial geometric imperfection measurements have also been performed and are reported in detail. The influence of the spread of plasticity and strain hardening on the shift of the neutral axis and the ultimate load carrying capacity is also examined. Based on the obtained test results, the current design provisions of EN 1993-1-4 [1] for these types of cross-sections were assessed and found to be unduly conservative. The effect of strain hardening on the structural response of stocky stainless steel sections and the need to account for it in design has been highlighted.

1. Introduction

Owing to its favourable structural properties, excellent durability and aesthetic appeal, stainless steel is gaining increasing usage in the construction industry and has attracted considerable attention from researchers and practising engineers alike [2-4]. Previous experimental research on stainless steel components has been dominated by tests on cold-formed circular, square and rectangular hollow sections (CHS, SHS and RHS, respectively) and welded I-sections [5], with other cross-section types receiving less attention. Column and beam tests have been performed on stainless steel oval hollow sections (OHS) [6, 7], whilst tests on stainless steel non-doubly symmetric sections have been mainly focusing on angle [8], channel [8] and lipped channel sections [9-11] in compression. Recently, tests on stainless steel lipped channel section beams bent about their major axis have been conducted [12] to investigate the interaction between distortional and global buckling. When asymmetric sections are subjected to bending about an axis that is not an axis of symmetry, flexure induces different stresses at the extreme tensile and compressive extreme fibres and leads to a shift in neutral axis with the progression of plasticity. No test data on the cross-sectional response of stainless steel sections subjected to bending not about an axis of symmetry have been reported to date.

Current structural stainless steel design guidance [1] is concerned mainly with doubly symmetric sections, primarily tubular sections and I-sections, which are commonly employed in structural applications. However, mono-symmetric stainless steel sections and in particular angle sections are widely employed in a range of structural applications, to act as wind posts, lintels, truss chords, lattice towers, pipeline frames, retrofitting of current structures [14] and so on, due to their simple geometry and ease of fabrication of connections; hence their design is of considerable practical significance. The European structural design rules for bending rely essentially on the classification of cross-sections into discrete behavioural groups according to their element width-to-thickness ratios, as compared to specified slenderness limits set out in [1]. As reported in [5], these slenderness limits were derived on the basis of experiments on stainless steel stub columns and beams, conducted primarily on SHS, RHS and I-sections. The lack of relevant test data on non-doubly symmetric stainless steel sections means that the current design provisions in EN 1993-1-4 (2006) [1] rely solely on assumed analogies with structural carbon steel and do not account for the special features of stainless steel, namely its rounded stress-strain response and pronounced strain hardening. Neglecting

the high degree of strain hardening has been shown to lead to overly conservative ultimate capacity predictions [5, 13] particularly for stocky cross-sections in bending. However, the effect of the nonlinear material behaviour of stainless steel on the structural response of non-doubly symmetric cross-sections in bending has not been studied to date. Given that beyond the elastic limit a shift in neutral axis occurs due to the spread of yielding throughout the cross-section and the high shape factors often associated with non-symmetric sections, it is expected that the effect of the rounded material stress-strain behaviour on the structural response will be even more pronounced for non-doubly symmetric cross-sections in bending.

To address these issues, an experimental study into the structural response of mono-symmetric and asymmetric sections in bending has been carried out. A total of 16 beam tests were conducted in both the 3-point and 4-point bending configurations (8 tests in each). Tensile coupon tests and initial geometric imperfection measurements have also been performed and are reported herein. Based on the obtained results, the current design provisions of EN 1993-1-4 [1] were evaluated and found to be safe, but excessively conservative over the full local slenderness range.

2. Literature review

Although there has only been limited research on stainless steel angles and channels in bending, there has been extensive work conducted on these sections made of structural carbon steel. A brief review of the previous research, with an emphasis on an angle sections, is given in this section.

Trahair studied analytically [15] the behaviour of single angles with different loading and restraint conditions in a series of papers recognizing the complexity that they present due to the lack of double symmetry and the coexistence of flexure, torsion and shear in many cases. Initially, design recommendations were developed for the classification and moment resistance calculation of laterally restrained angle sections subjected to biaxial bending [16], based on modifications to existing rules for I-section flange outstands, and reduction coefficients to account for the combined effect of torsion, shear and bearing were proposed [17]. Subsequently, based on large rotation analysis, design recommendations were proposed for unrestrained angle section beams subjected to major axis bending [18], biaxial bending [19], major axis bending and torsion [20] and biaxial bending and torsion [21]. In all cases

the material response was assumed to be elastic-perfectly plastic and slenderness limits were proposed, according to which either the elastic or the plastic moment resistance should be employed in design.

A series of numerical studies have been reported by Earls on slenderness limits and the ultimate moment resistance of single angle members, considering major axis bending [14], geometric axis bending inducing compression in the horizontal leg [22] and geometric axis bending inducing tension in the horizontal leg [23]. Based on the numerical results, design recommendations for slenderness limits and bracing requirements were made [24]. The focus of the research reported in [14, 22-24] was on determining local and global slenderness limits to enable the plastic moment resistance of an angle section beam to be achieved, but with no explicit account for strain hardening. The high conservatism embedded in the then applicable design guidance was highlighted and the findings of [24] were taken into account in the development of the latest version of the only structural design code dedicated exclusively to angle members [25].

The above numerical studies [14, 22-24] were validated against the tests reported by Madugula et al. [26], who investigated the flexural response of double-angle beams subjected to 3- and 4-point bending, which simulated laterally restrained single angles bent about their geometric axis. Both possible orientations of geometric axis bending (i.e. inducing tension or compression in the horizontal leg) were considered. The experiments revealed a high level of conservatism in structural design codes, as even the most slender cross-sections exceeded their plastic moment resistance. A similar experimental approach to that reported in [26] is followed in the present paper.

3. Experimental investigation

In order to address the lack of experimental data on stainless steel beams with non-doubly symmetric cross-sections, a series of tests has been conducted in the Structures Laboratory of the Department of Civil and Environmental Engineering at Imperial College London. The experiments were performed on austenitic stainless steel angles bent about their geometric axis and channel sections bent about their minor axis. Auxiliary tests on material coupons extracted from the same lengths of section as the test specimens and initial geometric imperfection measurements were also conducted and are reported herein.

3.1 Overview

All test specimens were provided by Montanstahl AG [27] and were laser-welded sections comprising hot-rolled stainless steel plates in Grades EN 1.4571, EN 1.4307 and EN 1.4404 [28]. Laser-welding is an efficient production method, which employs powerful lasers to locally melt and fuse together individual metallic components (solid, hollow or flat strips) of varying thicknesses and material grades into a range of complete structural sections, such as I-sections, T-sections, angles and channels, without the use of filler material. This technology has been used for the production of mild steel and stainless steel sections [27, 29]. Owing to the high precision of the laser beam, the heat input is kept to a minimum, thus resulting in very small heat affected zones, low thermal distortions and low residual stresses [29]. The weld seams are very small in comparison to traditional arc welding processes, resulting in sections featuring essentially sharp edges and corners [27], as shown in Fig. 1. Hence the weld sizes were neglected in this study and it was assumed that all sections comprise plated elements with sharp corners.

A total of 3 channel and 2 angle cross-section geometries was considered. The channels were subjected to 3-point and 4-point bending in both possible orientations (i.e. inducing compression in the web (the 'n' bending orientation) and inducing tension in the web (the 'u' bending orientation)), resulting in a total of 12 tests on channel sections. The 2 angle sections considered were also subjected to 3-point and 4-point bending about their geometric axis inducing compression in the shorter leg, resulting in 4 tests in total. The geometries of the tested simply-supported beam specimens were measured prior to testing and are reported in Tables 1 and 2 for the angle sections and channel sections respectively, where the total specimen length, as well as the span length between the supports is also reported. The adopted symbols for the cross-section geometry are defined in Fig. 2. Regarding the specimen designation, an "A" or "C" refers to an angle or a channel specimen; this is followed by the nominal cross-section dimensions and the number 3 or 4 to signify 3-point or 4-point bending, respectively. Since the angle sections were tested in pairs of nominally identical specimens, mean values of the paired angles are reported. The geometric proportions of the tested sections were such that they cover over all 4 cross-section classes [1] to allow a thorough investigation of the structural response of mono-symmetric sections over a wide range of local slendernesses.

3.2 Tensile coupon tests

Tensile tests on coupons extracted from the middle part of the plates of the finished cross-sections were conducted according to [30], to obtain the basic material response and to facilitate the analysis of the subsequent test results. The tests were carried out in an INSTRON 250 kN machine with an initial strain rate of 0.00001 s^{-1}, increasing after the attainment of the 0.2% proof stress to 0.00007 s^{-1} up until the attainment of the 1.0% proof stress and then increasing to 0.00025 s^{-1} thereafter until failure. The key material properties, namely the Young's modulus E, the 0.2% proof stress f_y, the 1% proof stress $f_{1.0}$, the ultimate tensile stress f_u, the strain at the ultimate tensile stress ε_u, the strain at fracture over the standard gauge length [30] ε_f and the Ramberg-Osgood parameters n and $n_{0.2,1.0}$ [31-33], which are a measure of the nonlinearity of the material response, are reported in Table 3. For the channel sections made up of plates of dissimilar thicknesses t, tensile tests on coupons extracted from both the flange and the web were conducted and labelled W and F for the web and flange respectively. The respective mill certificate values are given in Table 4, where the material grade of the stainless steel plates making up the test specimens is also reported. It can be observed that the experimentally obtained 0.2% proof stress is, on average, slightly below the corresponding mill certificate value. This is attributed to the effect of the strain rate on the material response [34], with mill tests typically conducted at higher strain rates than those used in the laboratory. It should be noted that the experimentally determined stress values are static values and were obtained by pausing the tensile tests for 2 minutes when approaching the 0.2% and 1% proof stresses and the ultimate stress and hence incorporate the static drop attributed to stress relaxation, which is commonly observed in similar tests [34]. All tested coupons exhibited very high ductility, with strains at fracture ε_f in excess of 60%.

3.3 Initial geometric imperfection measurements

Local initial geometric imperfections were measured along a 600 mm length of each tested section size, following the procedure reported in [35]. The specimens were firstly secured to the flat bed of a milling machine. A displacement transducer, which was attached to the head

of the milling machine, was then moved along the central 600 mm of the specimens, recording displacements at 20 mm intervals along the locations shown in Fig. 3 to obtain a representative local imperfection pattern for each constituent plate element. As shown in Fig. 3, measurements were taken along 2 lines for the outstand elements, namely along the supported edge and along the free edge, whilst for the internal plate elements, measurements were taken along the two supported edges and along the centreline of the supported element. The datum line, deviations from which were considered to be local imperfections, was assumed to be a best fit line through the points measured in the vicinity of the nodal lines (i.e. the lines at which the various plated elements intersect with one another) of the specimens. The maximum measured values of the local imperfections measured along each plate and the overall maximum value w_0 are reported in Table 5, where w_{fl1}, w_{fl2} are the maximum imperfections recorded for each of the flanges (w_{fl1} corresponds to the longer leg for the angle sections) and w_{web} is the maximum recorded imperfection for the channel web. Given the effect of the fabrication process on the geometric imperfections and the lack of reported local imperfection data for laser welded stainless steel sections in the literature, these data can be used in the future validation of numerical models.

3.4 Experimental setup and instrumentation

All specimens were tested in both the 3-point and the 4-point bending configuration. All tests were conducted using displacement control with a crosshead movement rate of 3 mm/min. For the 3-point bending tests, a concentrated load was applied at mid span, whilst 2 loads were applied via a spreader beam at third-points in the 4-point bending arrangement. The specimens had a span-to-height ratio of between 15 and 20, which was considered to be representative of the proportions of practical structural members and sufficiently high for the specimens to exhibit a primarily flexural behaviour with negligible influence from shear. All specimens overhung the end supports by 50 mm and 25 mm thick plates were employed to spread the load at the loading points and at the support locations (i.e. 3 plates for the 3-point bending and 4 plates for the 4-point bending), which were affixed to the specimens by means of bolting and clamping. The bolt sizes were limited to 6 mm, as this size was deemed sufficiently small not to affect the cross-sectional response and were located near the elastic neutral axis, where the influence of the bolt holes on the cross-section response would be minimal.

For the angle specimens, two nominally identical angle sections were paired with the aid of 25 mm thick spacer plates, as schematically shown in Fig. 4 and were subjected to geometric axis bending (i.e. bending about an axis parallel to one of the angle legs) similarly to the sections studied in [22, 23, 26]. The spacer plates had a width equal to two times the inner leg width plus an additional 50 mm (i.e. 2(b-t)+50 mm) and a height equal to h-t. In this case, the plates served the additional purpose of forming a compound member with increased out-of-plane stiffness thus resisting the occurrence of lateral torsional buckling. Moreover, the presence of the spacer plates, which are shown schematically in Fig. 5 for the 3-point bending configuration, facilitates the application of loading through the spacer plates without inducing torsion. For the channel specimens the plates were mainly utilized to locally strengthen the test specimens at the locations of concentrated load application, hence mitigating against local bearing failure.

The employed instrumentation comprised a load cell to measure the applied load, one inclinometer at each end of the specimens to measure end rotations, and LVDTs at the loading points and at mid-span to measure vertical deflections. One LVDT was employed for the 3-point bending tests to obtain the mid-pan deflection and 3 LVDTs were employed for the 4-point bending tests, thus allowing both the maximum deflection and the curvature in the constant moment region to be monitored. Six strain gauges were affixed to the angle specimens (3 per angle section) and three strain gauges were affixed to the channel specimens to allow the monitoring of the position of the neutral axis. The strain gauges were located at the flange tips and at the middle of the web for the channel sections and at the flanges tips and the corner of the section for the angle specimens, as shown in Fig. 6. The distance between the centreline of the strain gauges and the tip of the section plate on which they were affixed was 10 mm. With respect to the specimen length, the strain gauges were located at a distance of 50 mm from mid-span for the 3-point bending tests and at mid-span for the 4-point bending tests.

Fig. 7 depicts the experimental setup and the employed instrumentation for a typical 3-point bending test on a channel specimen. All data were recorded at 2 second intervals and the full load-deformation histories of the test specimens were captured. The results are presented and discussed in the following section.

4. Results and discussion

4.1 Behaviour of angle specimens and assessment of EN 1993-1-4 provisions

The behaviour of the tested angles is first discussed in the section, after which the provisions of EN 1993-1-4 are assessed. All tested angle specimens exhibited significant inelastic deformations in the plane of loading, followed by failure through local buckling. The deformed test specimens are shown in Fig. 8. In the 4-point bending configuration, local buckling occurred over a single half-wavelength between the loading points, whilst for the 3-point bending specimens, local buckling was confined to the vicinity of the loading point at mid-span, where the compressive stresses are higher due to the presence of the moment gradient.

The full load-deformation responses obtained from the tests are illustrated for all angle specimens in non-dimensional format in Fig. 9. The experimentally obtained moment at mid-span M is normalized by the plastic moment resistance M_{pl} of the respective cross-section, which is computed on the basis of the experimentally determined nominal yield stress f_y and measured geometric cross-section properties. For specimens loaded in the 3-point bending configuration, the average measured end rotation θ is normalized by the elastic rotation θ_{pl} corresponding to M_{pl}, whilst for the specimens subjected to 4-point bending the experimentally determined curvature is normalized by the elastic curvature κ_{pl} corresponding to M_{pl}. All specimens initially exhibit a linear response. Both angle specimens loaded in the 4-point bending configuration can be seen to comfortably exceed their plastic moment resistance and to exhibit excellent deformation capacity as they maintain their moment resistance throughout very large inelastic deformations. The 3-point bending specimens can be seen to reach even higher moment resistances than their 4-point bending counterparts but possess lower deformation capacity.

It should be noted that failure of one of the bolts connecting the individual angle members of specimen A100×65×11-3 to the spacer plate occurred during testing, though this occured at high inelastic in-plane deformations, as can be seen in Fig. 9, and is therefore believed not to have had a significant effect on the recorded ultimate load. However the bolt failure is believed to have had an effect on the deformation at which the failure load occurred.

All key experimental results obtained from the tests on the angle specimens are summarized in Table 6. These include the width-to-thickness ratio c/tε of the two legs of the angles, which is the slenderness parameter adopted in EN 1993-1-4 [1], the corresponding element class (with the leg of the angle in pure compression being more critical than that in bending), the experimental ultimate moment M_u, the experimental ultimate moment normalized by the elastic moment resistance M_{el}, plastic moment resistance M_{pl} and Eurocode predicted resistance M_{EC3}, as well as the deformation capacities R_m and R_u which are defined in Eqs. (1) and (2) and in Fig. 10.

$$R_m = \frac{\theta_m}{\theta_{pl}} - 1;\ R_m = \frac{\kappa_m}{\kappa_{pl}} - 1 \quad (1)$$

$$R_u = \frac{\theta_u}{\theta_{pl}} - 1;\ R_u = \frac{\kappa_u}{\kappa_{pl}} - 1 \quad (2)$$

where θ_m and κ_m are the rotation and curvature values corresponding to the ultimate moment and θ_u and k_u are rotation and curvature values when the moment-deformation curve drops down to M_{pl} after the attainment of the ultimate moment. Hence R_m is the plastic part of the deformation corresponding to the ultimate load, whilst R_u is the plastic part of the deformation when the moment decreases to M_{pl} following the attainment of the ultimate moment as shown in Fig. 10. The reason for reporting both deformation capacities lies in the fact that in most cases the test had to be terminated due to excessive deformation prior to the attainment of R_u. In these cases, the reported R_u values are the maximum recorded values prior to unloading of the specimen, and are indicated with a '>' sign in Table 6.

EN 1993-1-4 [1] does not provide any specific guidance for the design of angle sections in bending and sets out the familiar cross-section classification process to assess the effect of local buckling on their cross-sectional resistance and determine the appropriate moment resistance. Given that the aspect ratio (i.e. M_{pl}/M_{el}) of angle sections is considerably larger (approximately 1.8 for the tested angle sections) than the aspect ratio of typical I-sections, SHS, RHS and CHS, on which previous research has focused, the effect of cross-section classification on the design resistance is more significant. It should also be noted that even though a Class 1 limit is specified for stainless steel sections, plastic design is currently not permitted for stainless steel structures, despite the high ductility exhibited by stocky stainless steel cross-sections and some encouraging results from recent studies [36]. Nonetheless the deformation capacity of R=3, which is generally used as the minimum required value for

plastic design of steel structures [37], can serve as a benchmark value against which the test results reported herein can be assessed.

From Table 6 and Fig. 9 it can be seen that despite the significant difference in terms of local plate slenderness of the tested angle specimens (A50×50×4 is classified as Class 4, whilst A100×65×11 is classified as Class 1), the observed behaviour and recorded normalised ultimate test moments (M_u/M_{pl}) are similar. However the ultimate capacity predictions of EN 1993-1-4 [1] vary considerably due to the different classes to which the tested sections are assigned. For specimens loaded in the 4-point bending configuration, EN 1993-1-4 [1] underestimates the resistance of the Class 1 section by 10%, whilst the Class 4 section is predicted to reach less than half of its actual ultimate moment. The code becomes even more conservative for the specimens tested in 3-point bending, highlighting the importance of the moment gradient. The effect of the moment gradient on the structural response of both the angles and channels is discussed further in Section 4.3.

4.2 Behaviour of channel specimens and assessment of EN 1993-1-4 provisions

The behaviour of the tested channels is first discussed in the section, after which the provisions of EN 1993-1-4 [1] are assessed. Typical failure modes of the tested channel specimens are depicted in Figs 11 and 12 for channels subjected to bending inducing compressive stresses in the web and tensile stresses in web respectively. Similar to the angle specimens, the channels underwent significant inelastic deformations prior to failing by local buckling, with the local cross-section deformations being more concentrated towards the point of maximum bending moment in the 3-point bending configuration, as can be seen in Fig. 12.

The load-deformation response of the tested sections is shown in non-dimensional form in Figs 13-15 for sections C40×40×5×5, C100×50×4×4 and C100×50×6×9 respectively. For each section 4 curves are depicted, each corresponding to a single loading arrangement (3- or 4-point bending) and orientation of bending (whether the web is subjected to compressive or tensile stresses). All 4 curves can be seen to overlap in the early stages of the response, where the material remains elastic and no evidence of local buckling is present. Similar to the response exhibited by the angle specimens, the channel specimens loaded in the 4-point

bending arrangement display an earlier loss of stiffness, lower ultimate resistance and increased deformation capacity compared to their 3-point bending counterparts. This is discussed in more detail in Section 4.3.

For both orientations ('n' and 'u') of minor axis bending, the response is very similar for the same loading configuration for the 2 stocky sections considered (i.e. C40×40×5×5 and C100×50×6×9). However, for the more slender section (C100×50×4×4), a pronounced effect of the orientation of bending can be observed in Fig. 14, where the specimens in which the web is subjected to compression display superior strength and deformation capacity compared to their counterparts in which the web is in tension and the outstand flange tips are compressed. This is because the section is more susceptible to local buckling and hence more slender is the latter orientation.

The key experimental results obtained from the channel tests are reported in Table 7, where all symbols are as previously defined. In both bending orientations, two of the tested sections were Class 1 according to EN 1993-1-4 [1], whilst the C100×50×4×4 specimen was Class 3. However, all the tested cross-sections failed at moments beyond their plastic moment resistance and displayed high deformation capacities. The suitability of the slenderness limits given in EN 1993-1-4 [1] can be assessed on the basis of Figs 16 and 17 for internal elements in pure compression (i.e. the 'n' bending orientation where the channel web is in uniform compression) and outstand elements under a stress gradient, with the flange tips in compression (i.e. the 'u' bending orientation), respectively. The Class 1 limit is not assessed herein, given that plastic design in not currently permitted in EN 1993-1-4 [1] for stainless steel structures, through note that all tested specimens had a rotation capacity R_u greater than 3.

In Fig. 16(a), the ultimate test moments M_u for the channels bent in the 'n' orientation are normalised by the calculated plastic moment capacities M_{pl} (based on measured geometric and material properties), with a value of M_u/M_{pl} greater than unity indicating that the requirements for Class 2 cross-sections are met, which all tested sections may be seen to have achieved. In Fig. 16(b), the ultimate test moments for the channels bent in 'n' orientation are normalised by the elastic moment capacity to assess the Class 3 slenderness limits. Again, all test data points comfortably exceed unity, showing that the existing slenderness limits are safe.

In Figs 17(a) and 17 (b), the corresponding graphs to Figs 16(a) and 16(b) are shown based on the results of the channels tested in the 'u' orientation, with the flange tips in compression. Similar findings are also observed. Note that in Fig. 17(a), the test data points have been located with respect to the element slenderness $\alpha c/t\varepsilon$, where c is the flat width of the outstand element and α is the proportion of the outstand in compression, calculated on the basis of the position of the plastic neutral axis. In Fig. 17(b), the stress gradient is allowed for through the buckling coefficient k_σ, based on the position of the elastic neutral axis.

Overall, in all cases, the codified design resistances are comfortably exceeded by all tested specimens due primarily to the pronounced strain hardening of stainless steel [5]. As in the case of the angle specimens, the design provisions of [1] are more conservative for members subjected to 3-point bending due to the beneficial effect of the moment gradient, as discussed in Section 4.3.

4.3 Influence of moment gradient

In Fig. 9 and Figs 13-15, a clear influence of the moment gradient on both the deformation capacity and the ultimate moment resistance of the tested angles and channels can be observed. Table 8 quantifies that effect for the tested sections. On average, specimens subjected to 3-point bending display 19% higher moment resistance and 46% lower deformation capacity than their 4-point counterparts. The effect of the moment gradient on the rotation capacity [38] and the moment resistance [39] is attributed to the fact that in the 3-point bending configuration restraint to local buckling in the most heavily loaded cross-section is afforded by the surrounding material which is subjected to lower stresses. Given the uncertainty associated with the location and magnitude of live loads and hence the range of possible shapes of bending moment diagram, the current approach to ignore the beneficial effect of the steepness of the bending moment diagram in structural design is considered to be warranted.

4.4 Shift of neutral axis

Unlike cross-sections bent about an axis of symmetry, cross-sections bent about an axis that is not one of symmetry experience different stresses on the tensile and the compressive fibres. If the cross-section is sufficiently stocky not to fail by local buckling prior to the attainment

of the elastic moment resistance M_{el}, the spread of yielding and corresponding stress redistribution causes a shift of the location of the neutral axis (NA). The position of the neutral axis has therefore been monitored throughout the tests performed in this study. Based on the readings of the strain gauges (schematically shown in Fig. 6) and assuming a linear strain distribution throughout the cross-section depth, the location of the NA has been determined. For elastic-perfectly plastic materials, the NA should initially overlap with the theoretical elastic neutral axis (ENA) location, whilst a shift towards the plastic neutral axis (PNA) location is expected after yielding and with increasing strain values. However, the influence of a rounded material response with strain hardening like that exhibited by stainless steels on the actual position of the neutral axis. y_{NA} and its evolution from the ENA towards the PNA has not been studied to date.

In Table 9 the theoretical locations of the ENA and the PNA, the distance between the two and the distance between the ENA and PNA normalized by the cross-section height (in the plane of bending) are reported for each of the tested cross-sections, where y_{el} and y_{pl} are the distances of the ENA and PNA respectively from the nearest extreme fibre (i.e. the shortest leg for the angle sections, and the web for the channel sections). From Table 9 it can be concluded that the ENA and the PNA are generally relatively close to each other compared to the overall section height.

The measured location of the neutral axis (based on the strain gauge readings) y_{NA} varies during the test, and it should be noted that the accuracy of the determination of the location of the NA is affected by possible errors in determining the exact location of the strain gauges, by flange curling which distorts the shape of the cross-section and by local flexure of the plates due to local buckling. In order to facilitate the comparison of the evolution of the neutral axis location, with increasing deformation for the various sections considered, the normalized position of the NA with respect to the ENA is defined in Eq. (3) as a proportion of the distance between the ENA and the PNA

$$\bar{y}_{NA} = \frac{y_{el} - y_{NA}}{y_{el} - y_{pl}} \tag{3}$$

In Figs 18-20, the evolution of the relative position of the NA with increasing cross-sectional deformation (measured as normalized rotation for the 3-point bending specimens and normalized curvature for the 4-point bending specimens) is depicted for the A100×65×11, the C100×50×4×4-n and the C100×50×6×9-u specimens respectively. As expected the position of the NA initially at the ENA location, and progresses from the ENA towards the PNA upon departure from the elastic response. However, contrary to cross-sections made of materials exhibiting elastic-perfectly plastic response, in stainless steel cross-sections the NA then tends to move back towards the ENA at high deformation values due to the positive slope in the strain hardening range of the material response.

5. Conclusions

A detailed account of a total of 16 bending tests on non-doubly symmetric stainless steel sections - 4 angles bent about their geometric axis and 12 channels bent about their minor axis, has been given. Both 3- and 4-point bending tests were conducted, whilst both possible orientations of minor axis bending were considered for the channel sections. In line with previous studies on carbon steel angles subjected to pure bending, this paper has highlighted that stainless steel angles and channel sections subjected to bending exhibit significant strain hardening that can be accounted for in design. The EN 1993-1-4 [1] capacity predictions were shown to be excessively conservative, since even the class 4 test specimens comfortably exceeded their plastic moment resistance. This is attributed to the significant strain hardening exhibited by stocky stainless steel sections in conjunction with the high shape factor associated with this type of cross-sections. The evolution of the shift of the neutral axis caused by stress redistribution upon departure of the material response from linearity has been monitored. It was determined that the neutral axis progresses rapidly from the theoretical elastic neutral axis location towards the plastic neutral axis location, whereupon it shifts back gradually towards the elastic neutral axis location, due to the rounded nature of the material response. Finally, in line with previous studies, the influence of the moment gradient (i.e. whether 3-point bending or 4-point bending) was shown to influence both the ultimate moment resistance and the deformation capacity of the tested sections, with specimens subjected to 3-point bending possessing higher moment resistance but lower deformation capacities compared to their counterparts under 4-point bending. Research is

underway to extend previous work [40-42] to incorporate the effects of strain hardening into the structural design of non-doubly symmetric stainless steel sections subjected to bending.

Acknowledgements

The supply of specimens and financial support from Montanstahl AG is very gratefully acknowledged. The authors would like to thank Ms Natasha Arsenopoulou, Mr Richard Erb, Mr Costas Kyprianou, Mr Bart Drazyk and Mr Gordon Herbert for their involvement in the experimental part of the project.

References

[1] EN 1993-1-4 (2006) Eurocode 3. Design of Steel Structures: Part 1-4: General rules-Supplementary rules for stainless steel. Brussels, European Committee for Standardization. CEN.

[2] Gardner L. (2005) The use of stainless steel in structures. Progress in Structural Engineering and Materials. 7(2), 45-55.

[3] Baddoo NR. (2008). Stainless steel in construction: a review of research, applications, challenges and opportunities. Journal of Constructional Steel Research 64(11), 1199–206.

[4] Gedge G. (2008). Structural uses of stainless steel - buildings and civil engineering. Journal of Constructional Steel Research. 64(11), 1194-1198.

[5] Gardner L. and Theofanous M. (2008) Discrete and continuous treatment of local buckling in stainless steel elements. Journal of Constructional Steel Research. 64 (11), 1207-1216.

[6] Theofanous M., Chan T.M. and Gardner L. (2009). Structural response of stainless steel oval hollow section compression members. Engineering Structures 31(4), 922-934.

[7] Theofanous M., Chan T.M. and Gardner L. (2009). Flexural behaviour of stainless steel oval hollow sections. Thin-Walled Structures 47(6-7), 776-787.

[8] Kuwamura H. (2003). Local buckling of thin-walled stainless steel members. Steel Structures 3, 191-201.

[9] Lecce M. and Rasmussen K.J.R. (2006). Distortional Buckling of Cold-Formed Stainless Steel Sections: Experimental Investigation. Journal of Structural Engineering 132(4), 497-504.

[10] Becque J. and Rasmussen K.J.R. (2009). Experimental investigation of local-overall interaction buckling of stainless steel lipped channel columns. Journal of Constructional Steel Research. 65 (8-9), 1677-1684.

[11] Rossi B., Jaspart J.P. and Rasmussen K.J.R. (2010). Combined Distortional and Overall Flexural-Torsional Buckling of Cold-Formed Stainless Steel Sections: Experimental Investigations. Journal of Structural Engineering 136(4), 354-360.

[12] Niu S., Rasmussen K.J.R. and Fan F. (2014). Distortional–global interaction buckling of stainless steel C-beams: Part I - Experimental investigation. Journal of Constructional Steel Research 96, 127-139.

[13] Gardner L. and Nethercot D.A. (2004). Experiments on stainless steel hollow sections - Part 2: Member behaviour of columns and beams. Journal of Constructional Steel Research 60 (9), 1319-1332.

[14] Earls C.J. (1999) On single angle major axis flexure. Journal of Constructional Steel Research. 51 (2), 81-97.

[15] Trahair N.S. (2007). Behaviour of Single Angle Steel Beams. Research report: No R884. Centre for Advanced Structural Engineering, University of Sydney, Australia.

[16] Trahair, N. (2002) Moment capacities of steel angle sections. Journal of Structural Engineering. 128 (11), 1387-1393.

[17] Trahair, N. (2002) Bearing, shear, and torsion capacities of steel angle sections. Journal of Structural Engineering. 128 (11), 1394-1398.

[18] Trahair, N. (2003) Lateral buckling strengths of steel angle section beams. Journal of Structural Engineering. 129 (6), 784-791.

[19] Trahair, N. (2004) Biaxial bending of steel angle section beams. Journal of Structural Engineering. 130 (4), 554-561.

[20] Trahair, N. (2005) Buckling and torsion of steel equal angle beams. Journal of Structural Engineering. 131 (3), 467-473.

[21] Trahair, N. (2007) Biaxial bending and torsion of steel equal angle section beams. Journal of Structural Engineering. 133 (1), 78-84.

[22] Earls C.J. (2001) Geometric axis compactness criteria for equal leg angles: horizontal leg compression. Journal of Constructional Steel Research. 57 (4), 351-373.

[23] Earls C.J. (2001). Single angle geometric axis flexural compactness criteria: Horizontal leg in tension. Journal of Structural Engineering. 127 (6), 616-624.

[24] Earls, C. & Galambos, T. (1997) Design recommendations for equal leg single angle flexural members. Journal of Constructional Steel Research. 43 (1), 65-85.

[25] American Institute of Steel Construction. (2000). Load and resistance factor design of single-angle members. Chicago: American Institute of Steel Construction, Inc.

[26] Madugula, M. K., Kojima, T., Kajita, Y. & Ohama, M. (1996) Geometric axis bending strength of double angle beams. Journal of Constructional Steel Research. 38 (1), 23-40.

[27] EN 10088-1 (2005). Stainless steels - Part 1: List of stainless steels. Brussels, European Committee for Standardization. CEN.

[28] Montanstahl AG, "Manufacturing Technologies - Laser Fusion", [Online] Available from: http://www.montanstahl.com/products/technologies/?SID=1, 2009.

[29] Landolfo R., Mammana O., Portioli F., Di Lorenzo G. and Guerrieri M.R. (2008). Laser welded built-up cold-formed steel beams: Experimental investigations. Thin-Walled Structures 46 (7-9), 781-791.

[30] EN ISO 6892-1. (2009). Metallic materials – Tensile testing. Part 1: Method of test at room temperature. Brussels, European Committee for Standardization, CEN.

[31] Mirambell E. and Real E. (2000). On the calculation of deflections in structural stainless steel beams: an experimental and numerical investigation. Journal of Constructional Steel Research 54 (1), 109-133.

[32] Rasmussen K.J.R. (2003). Full-range stress-strain curves for stainless steel alloys. Journal of Constructional Steel Research 59(1), 47-61.

[33] Gardner L. and Nethercot D.A. (2004). Experiments on stainless steel hollow sections - Part 1: Material and cross-sectional behaviour. Journal of Constructional Steel Research 60 (9), 1291-1318.

[34] Huang Y. and Young B. (2014). The art of coupon tests. Journal of Constructional Steel Research 96, 159-175.

[35] Schafer B. and Peköz T. (1998) Computational modeling of cold-formed steel: characterizing geometric imperfections and residual stresses. Journal of Constructional Steel Research 47(3), 193-210.

[36] Theofanous M., Saliba, N., Zhao, O. and Gardner, L. (2014). Ultimate response of stainless steel continuous beams. Thin-Walled Structures 83, 115-127.

[37] Sedlacek G., Feldmann M. (1995). The b/t ratios controlling the applicability of analysis models in Eurocode 3, Part 1.1. Background Document 5.09 for chapter 5 of Eurocode3, Part1.1, Aachen.

[38] Kuhlmann, U. (1989). Definition of flange slenderness limits on the basis of rotation capacity values. Journal of Constructional Steel Research 14(1): 21-41.

[39] Ricles J.M., Sause R. and Green P.S. (1998). High-strength steel: implications of material and geometric characteristics on inelastic flexural behaviour. Engineering Structures 20(4-6), 323-335.

[40] Ashraf, M., Gardner, L. and Nethercot, D.A. (2006). Compression strength of stainless steel cross-sections. Journal of Constructional Steel Research. 62(1-2), 105-115.

[41] Gardner, L. (2008). The Continuous Strength Method. Proceedings of the Institution of Civil Engineers - Structures and Buildings. 161(3), 127-133.

[41] Afshan, S. and Gardner, L. (2013). The continuous strength method for structural stainless steel design. Thin-Walled Structures. 68, 42-49.

Experimental study of stainless steel angles and channels in bending

M. Theofanous[a], A. Liew[b] and L. Gardner[c]

Response to reviewers' comments

The authors would like to thank the reviewers for their constructive comments, which are given below in *italics*. Below each of the reviewers' comments are the responses and actions taken by the authors in **bold** font. We believe we have addressed as comments in full.

Reviewers' comments:

The paper presents an experimental study on non-doubly symmetric stainless steel sections in bending. A series of 16 beam tests in bending and material tests on coupons from the specimens were conducted. Some minor considerations should be taken into account before the final print.

In Fig 1 it is recommended to change the order like in figure 2. Angle at the left.
The authors agree that this is more consistent and have now re-ordered the images, as recommended.

Table 2 appears in the text (page 5 line 36) before Table 1 (page 5, line 43).
This has been resolved in the revised manuscript.

Table 4. The Young's modulus from the mill certificates is not reported in Table 4.
The Young's modulus is not provided in mill certificates.

Page 11, line 31, add [1] after EN 1993-1-4.
This has been added, as requested.

Page 12, line 10, "Fig. 14" instead of "Fig. 15".
Yes, this has been corrected, as suggested.

Table 7. It would be useful to separate web (outstand elements) and flange (internal elements) class for the analysis of figures 16 and 17.
The classification of the elements has now been separated, as recommended.

Page 13, line 58, "plastic moment resistance" instead of "yield moment"
The authors are not referring to the plastic moment resistance here. We are referring to the yield moment (i.e. the elastic moment resistance). This has been clarified by changing the term yield moment to elastic moment resistance and adding the symbol M_{el}.

Page 15, line 39, add "axis" after "neutral".
Agreed; this has now been corrected.

The following points should also be taken into account:
In figures 13, 14 - it is not easy to distinguish the lines. Please, check and improve this.
Figures 9, 10, 13, 14, 15, 16, 17, 18, 19 and 20 have different dimensions and should be harmonized.
The dimensions of these graphs have now been harmonized, as recommended.

Figure

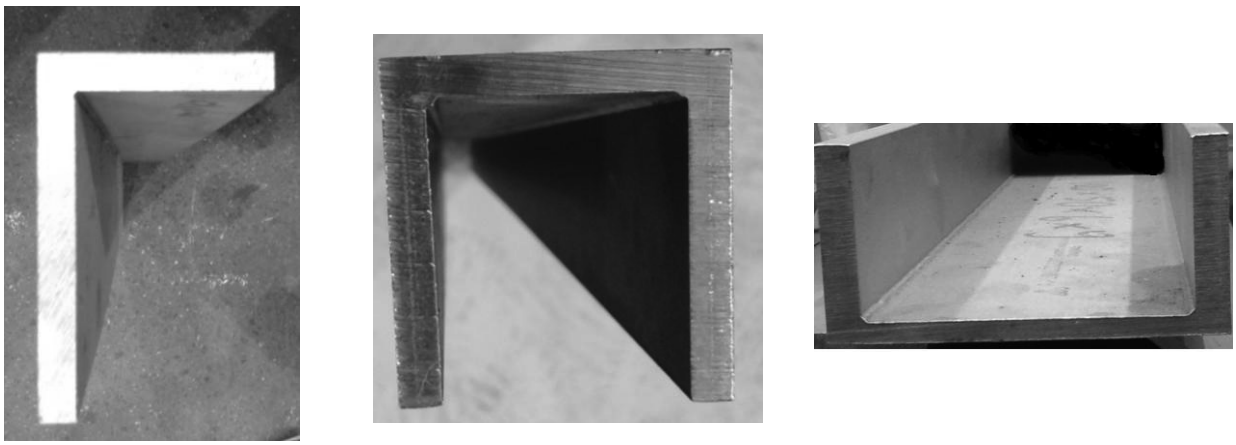

Fig. 1. Laser-welded cross-sections featuring essentially sharp corners.

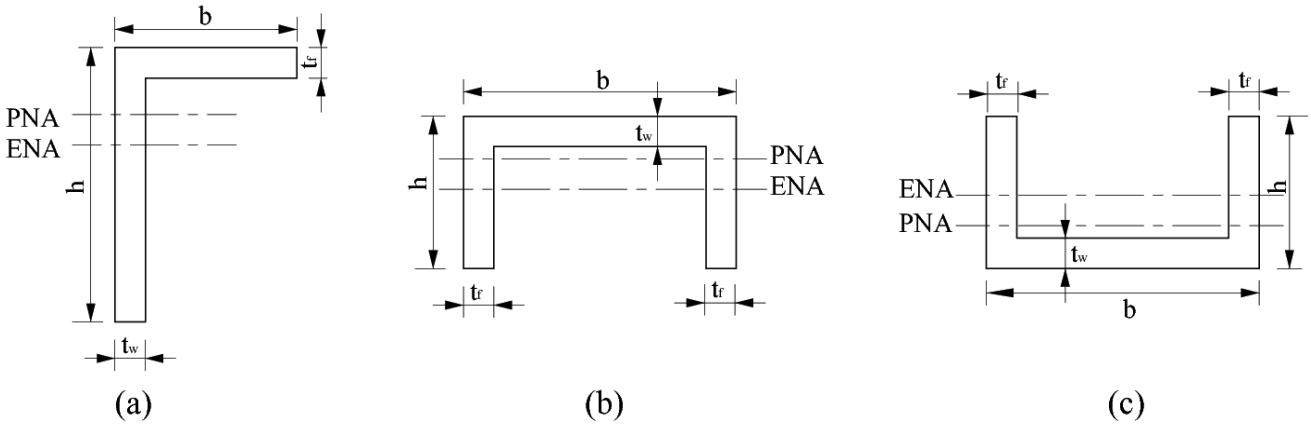

Fig. 2. Cross-section geometries of test specimens for (a) angle sections, (b) channels bent in the ‘n’ orientation and (c) channels bent in the ‘u’ orientation. ENA and PNA are the elastic and plastic neutral axes.

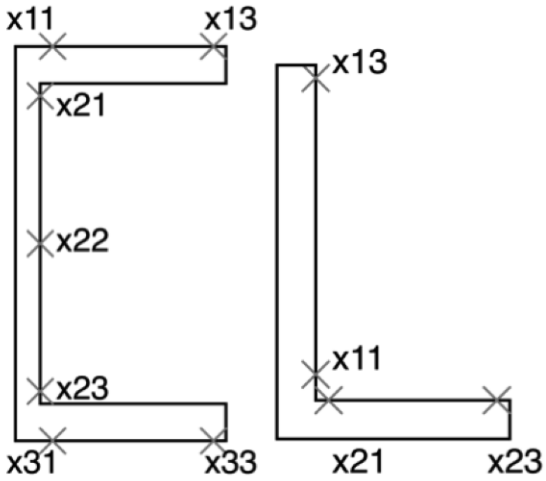

Fig. 3. Locations for initial local geometric imperfection measurements.

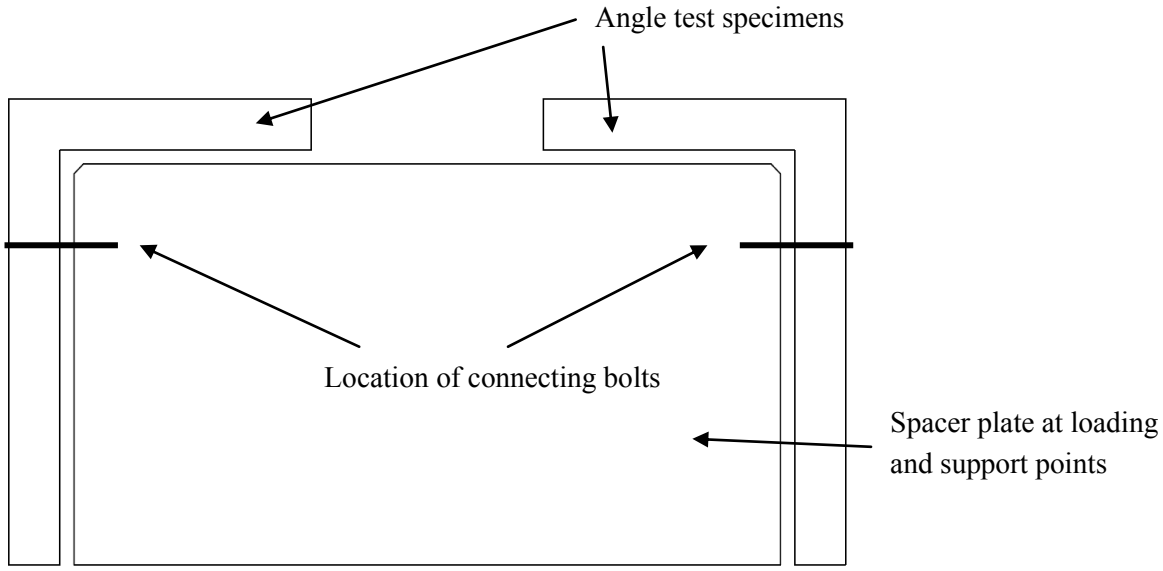

Fig. 4. Angles tested in pairs about their geometric axis.

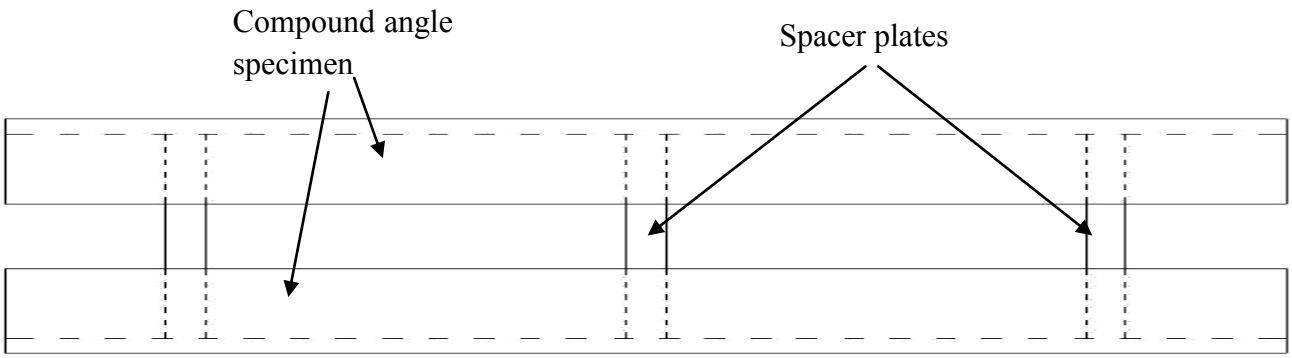

Fig. 5. Top view of double angle 3-point bending configuration

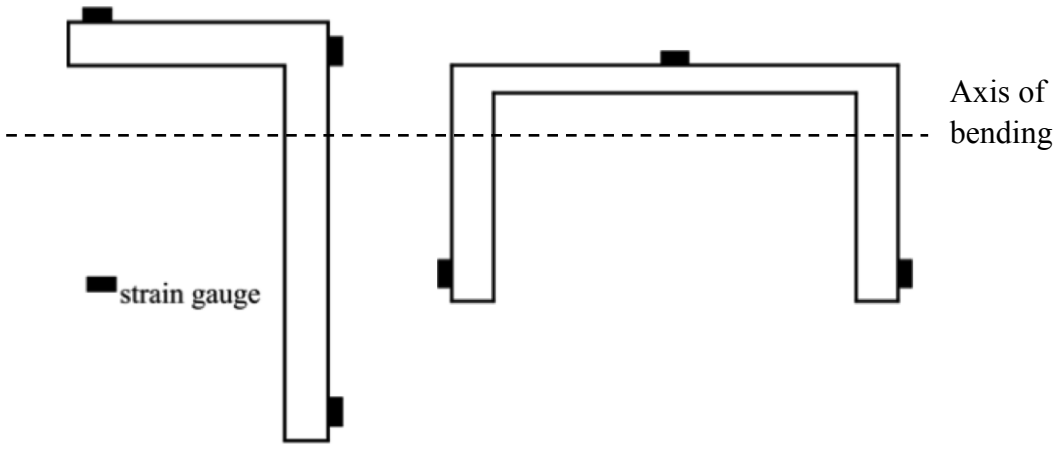

Fig. 6. Strain gauge locations.

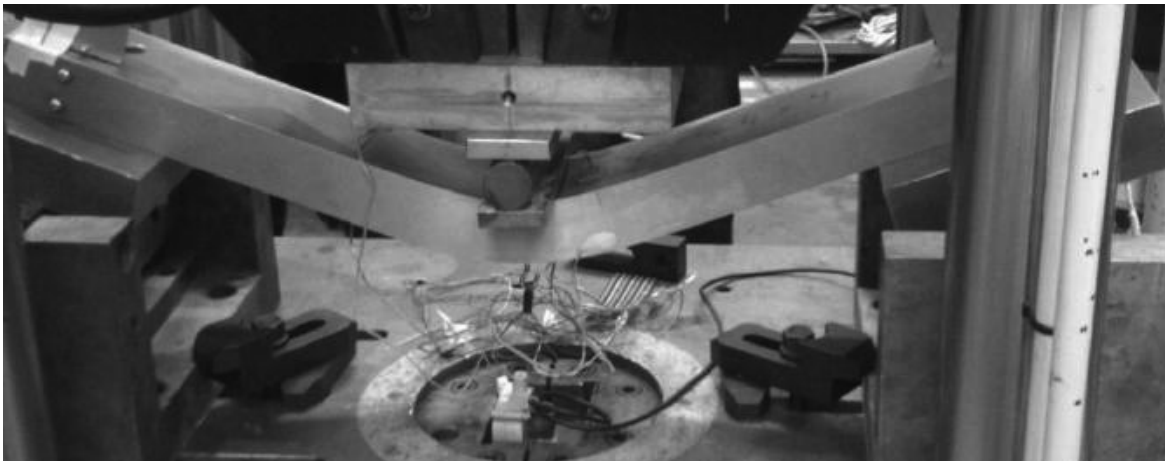

Fig. 7. Typical 3-point bending test setup.

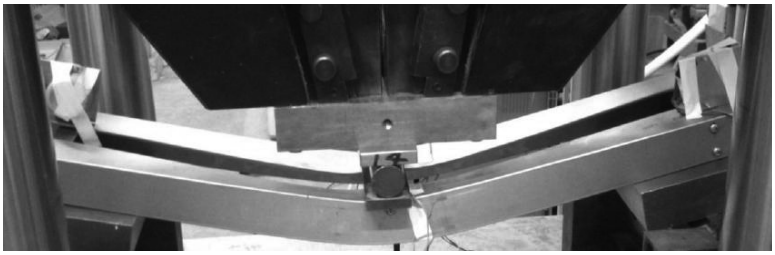

a) A 50×50×4-3

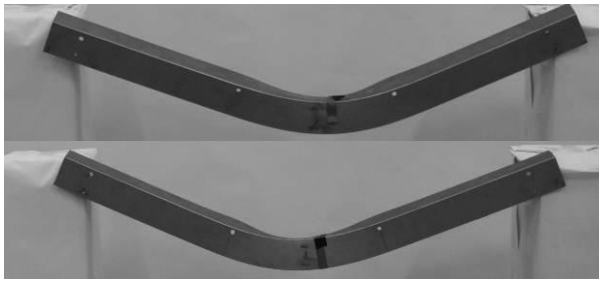

b) A 50×50×4-4

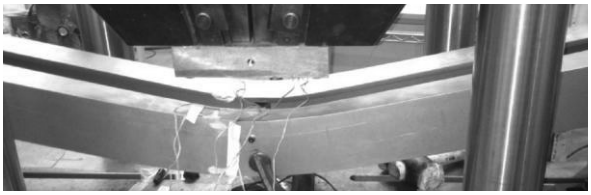

c) A 100×65×11-3

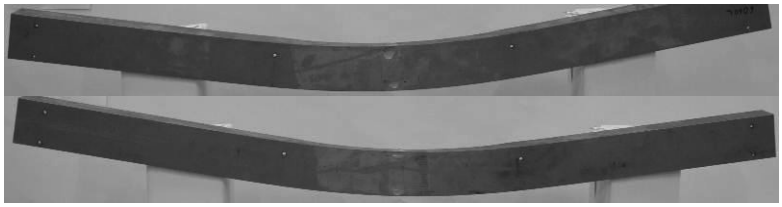

d) A 100×65×11-4

Fig. 8. Failure modes of tested angles: a) A 50×50×4-3 ; b) A 50×50×4-4;
c) A 100×65×11-3; d) A 100×65×11-4

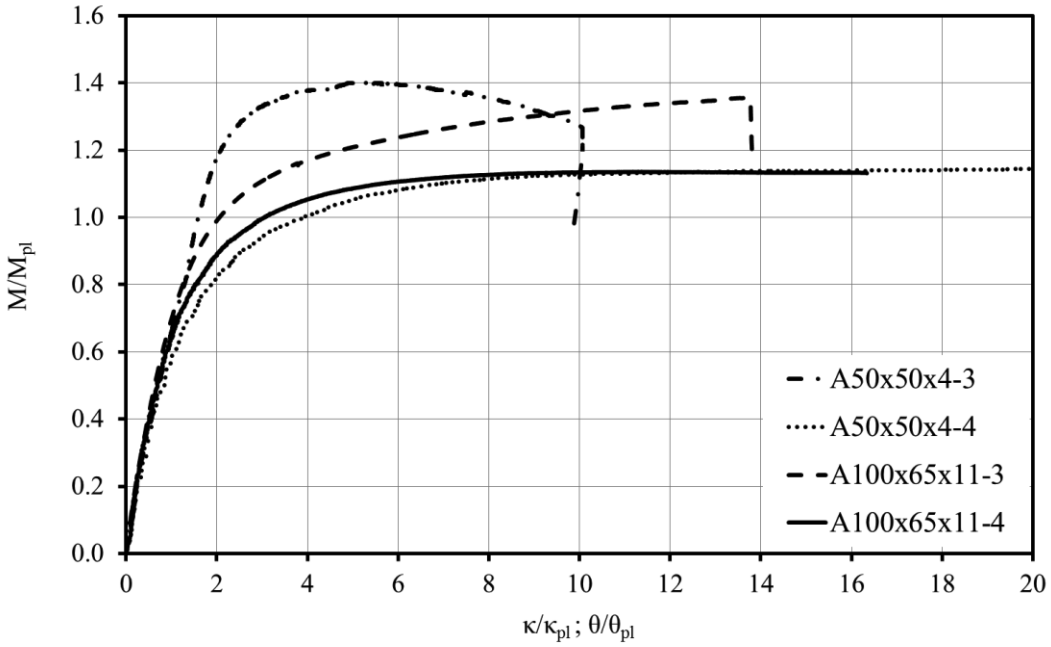

Fig. 9. Moment rotation and moment curvature curves of angle specimens.

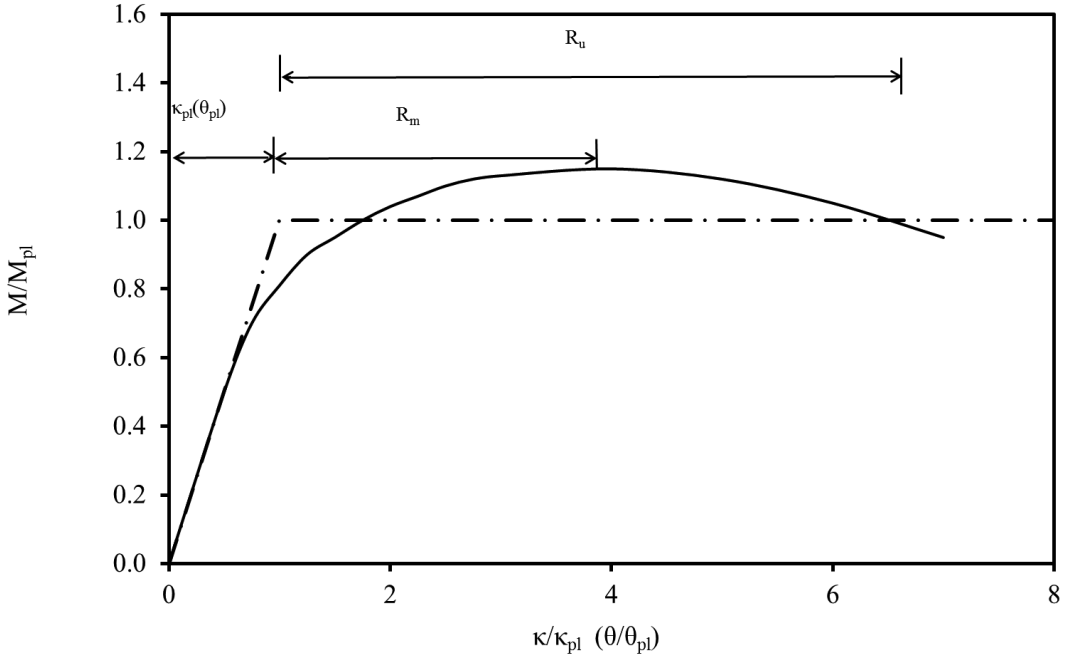

Fig. 10. Definition of deformation capacities R_m and R_u

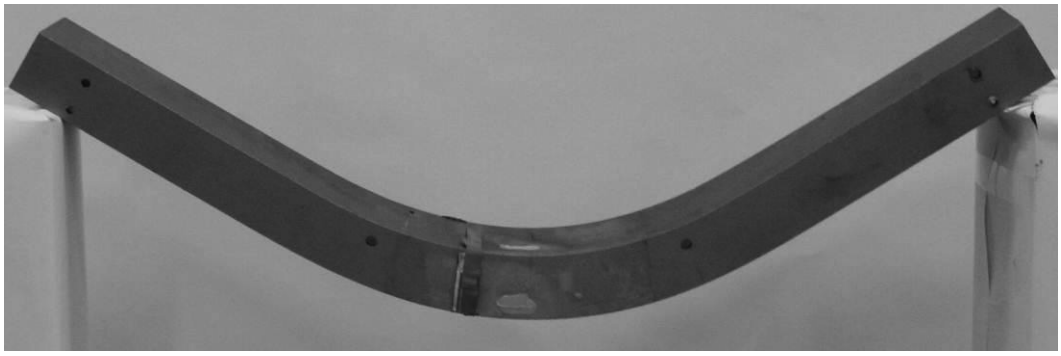

a) C 100×50×4×4-4-n

b) C100×50×6×9-3-n

Fig. 11. Failure modes of tested channels – web in compression:
a) C 100×50×4×4-4-n; b) C100×50×6×9-3-n

a) C 100×50×4×4-4-u

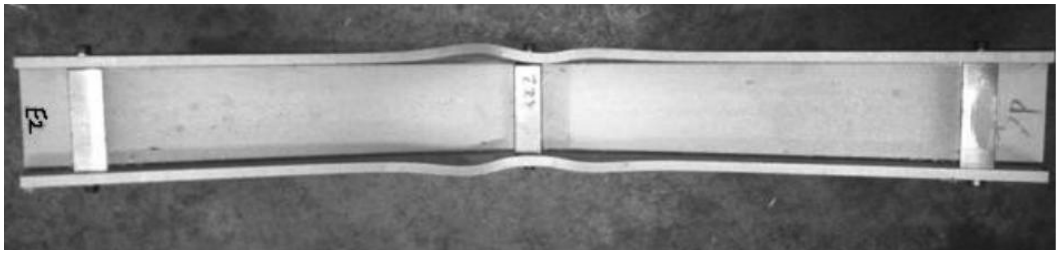

b) C100×50×6×9-3-u

Fig. 12. Failure modes of tested channels – web in tension:
a) C 100×50×4×4-4-n; b) C100×50×6×9-3-n

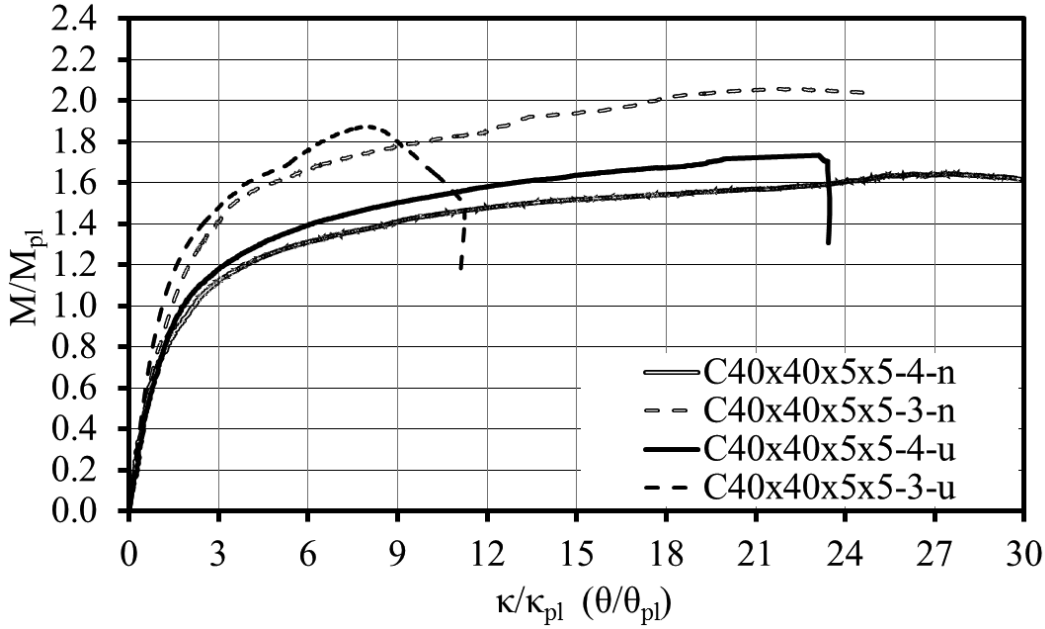

Fig. 13. Moment rotation and moment curvature curves of C 40×40×5×5 specimens.

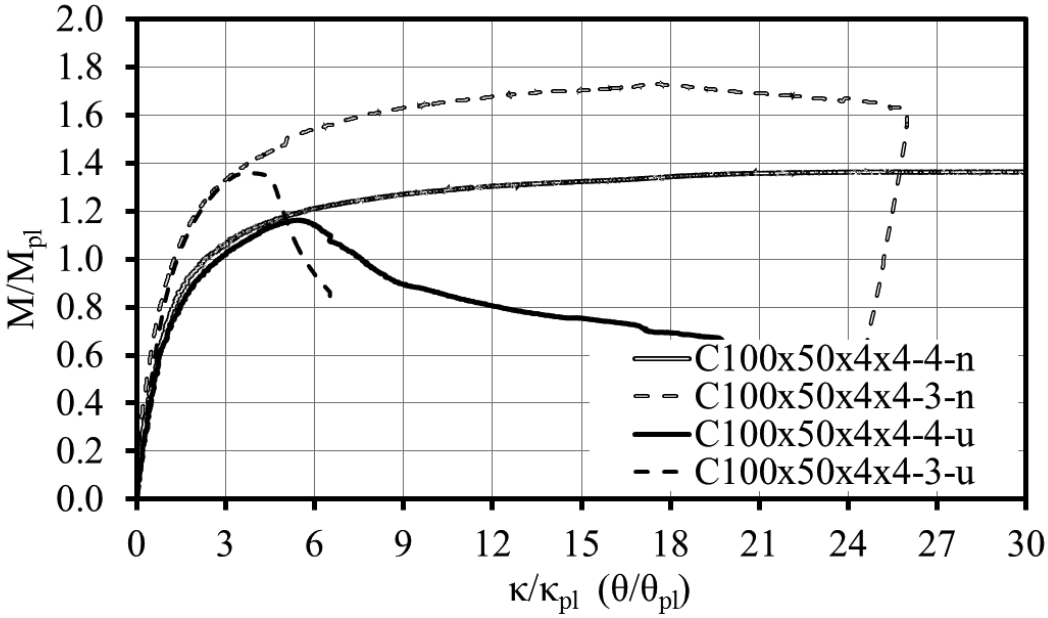

Fig. 14. Moment rotation and moment curvature curves of C 100×50×4×4 specimens.

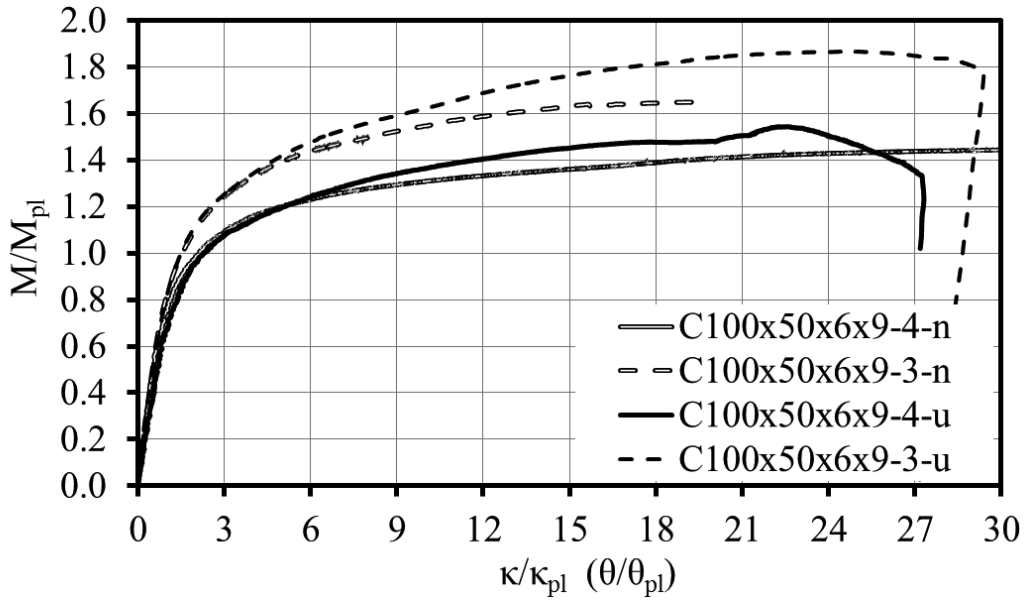

Fig. 15. Moment rotation and moment curvature curves of C 100×50×6×9 specimens.

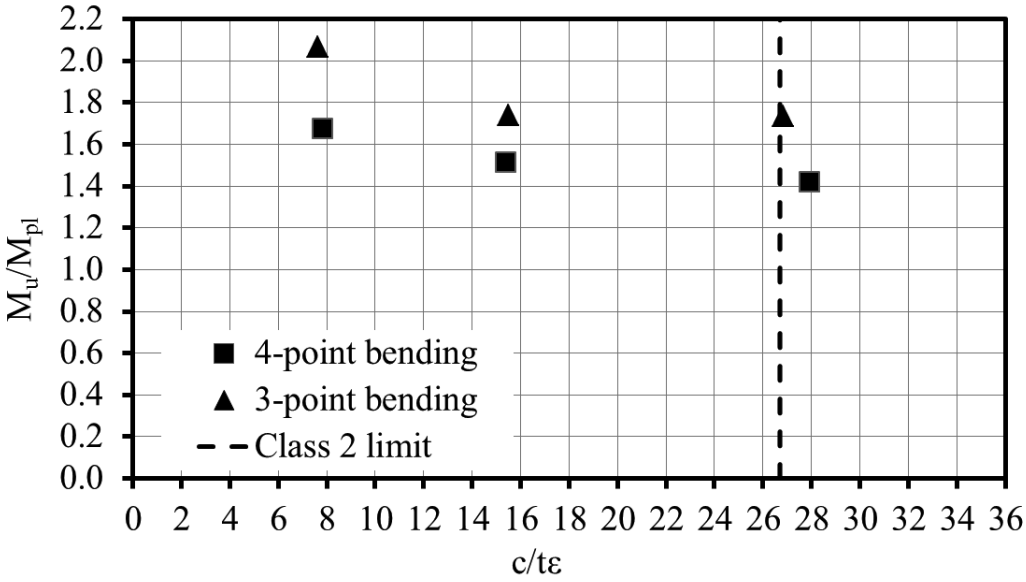

a) Class 2

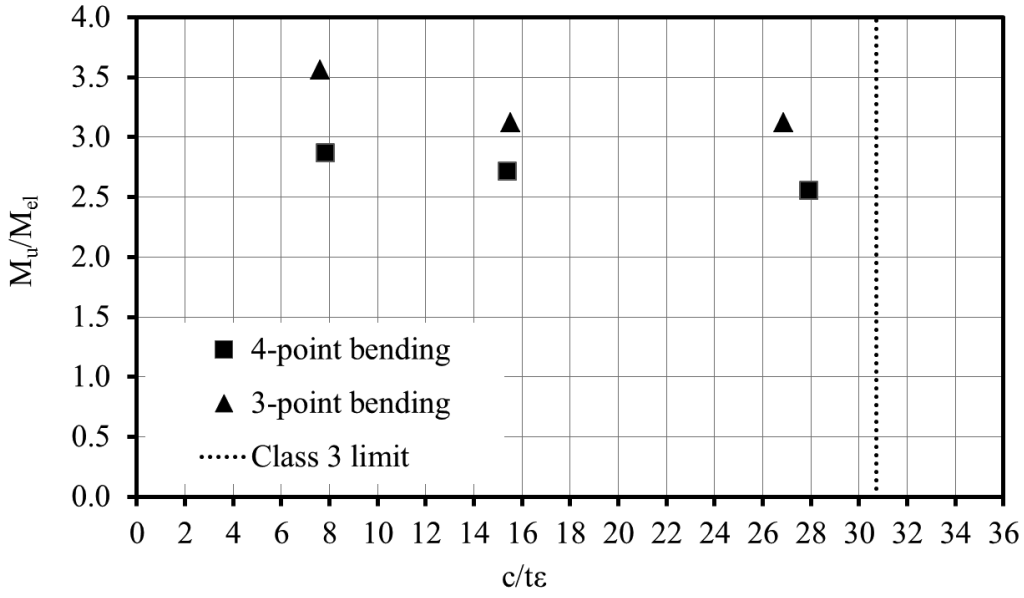

b) Class 3

Fig. 16. Assessment of slenderness limit for internal elements in compression: a) Class 2; b) Class 3.

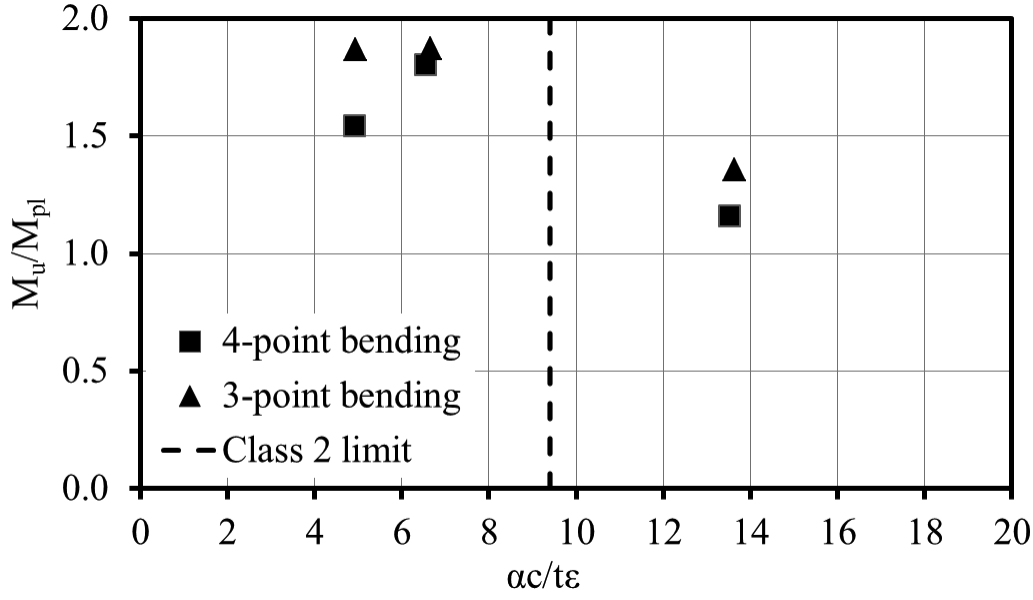

a) Class 2

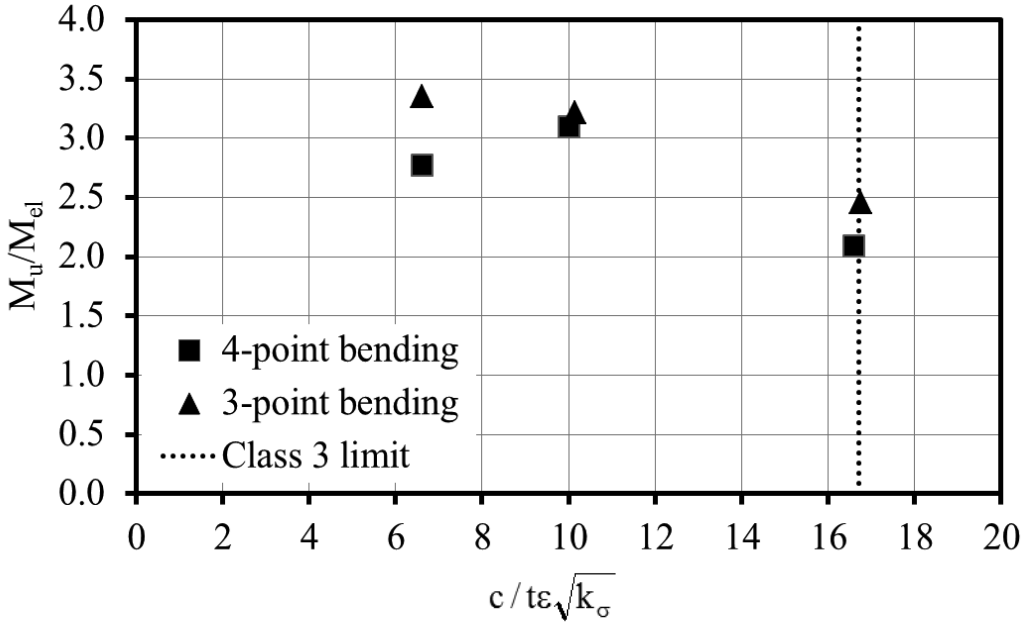

b) Class 3

Fig. 17. Assessment of slenderness limit for outstand elements subjected to bending: a) Class 2; b) Class 3.

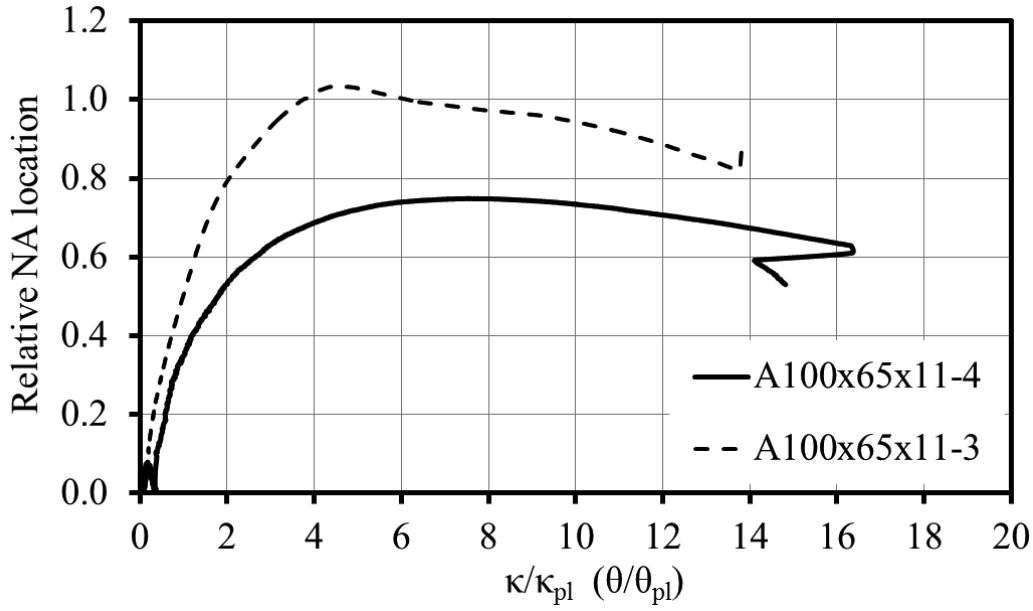

Fig. 18. Evolution of the location of NA with increasing deformation for the

A100×65×11 specimens.

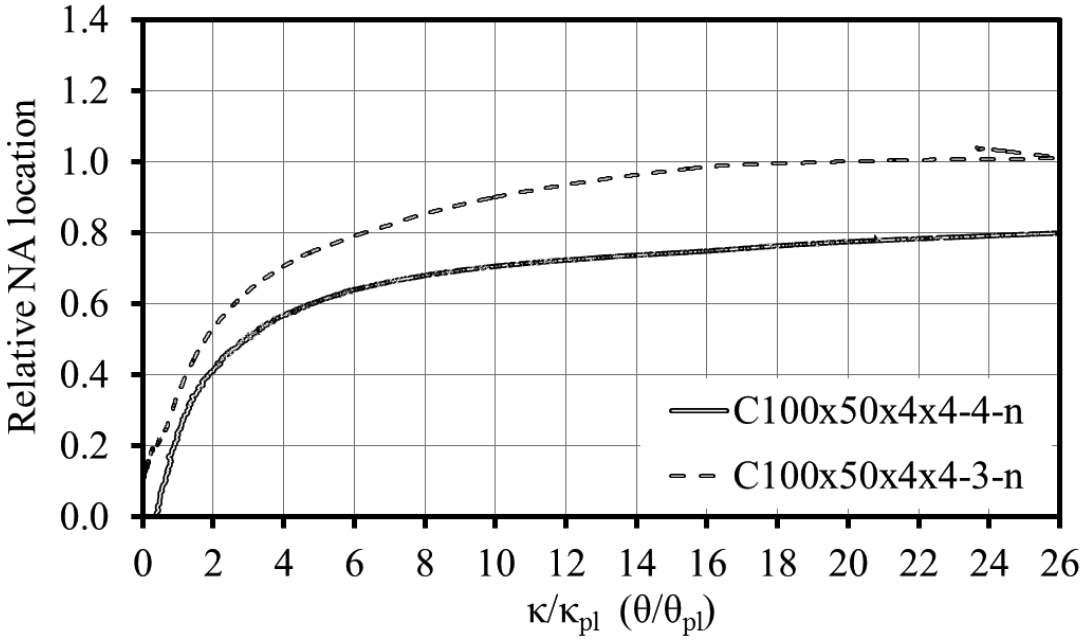

Fig. 19. Evolution of the location of NA with increasing deformation for the C100×50×4×4 specimens (web in compression).

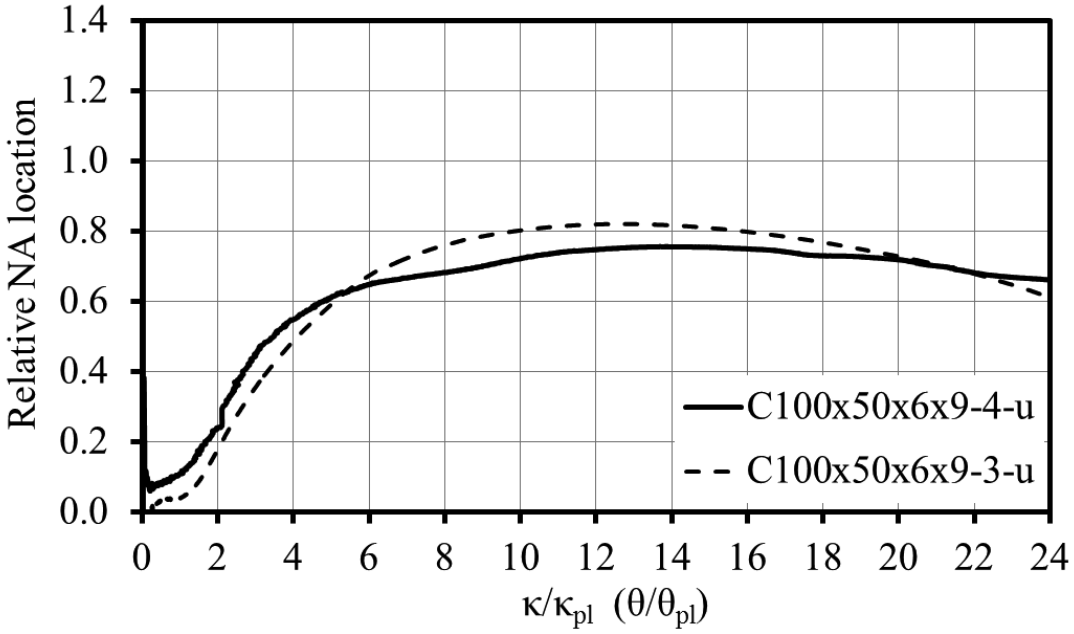

Fig. 20. Evolution of the location of NA with increasing deformation for the C100×50×6×9 specimens (web in tension).

Table 1: Geometry of tested angle specimens

Specimen	Testing configuration	Total length (mm)	Length between supports (mm)	b (mm)	h (mm)	t_f (mm)	t_w (mm)
A 50×50×4-3	3-point bending	849.5	750	50.53	50.45	4.14	4.17
A 50×50×4-4	4-point bending	849.3	750	50.70	50.49	4.16	4.18
A 100×65×11-3	3-point bending	1599.5	1500	65.11	99.46	10.70	10.66
A 100×65×11-4	4-point bending	1599.5	1500	64.95	99.71	10.62	10.63

Table 2: Geometry of tested channel specimens

Specimen	Testing configuration	Orientation	Total length (mm)	Length between supports (mm)	b (mm)	h (mm)	t_f (mm)	t_w (mm)
C 40×40×5×5-3-n	3-point bending	Web in compression	848	750	39.89	40.01	4.81	4.67
C 40×40×5×5-4-n	4-point bending	Web in compression	838	750	39.88	40.39	4.9	4.57
C 40×40×5×5-3-u	3-point bending	Web in tension	850	750	39.95	39.94	4.78	4.64
C 40×40×5×5-4-u	4-point bending	Web in tension	850	750	39.88	39.99	4.84	4.61
C 100×50×4×4-3-n	3-point bending	Web in compression	836	750	50.02	100.29	3.95	4.01
C 100×50×4×4-4-n	4-point bending	Web in compression	835	750	50.18	100.33	3.95	3.86
C 100×50×4×4-3-u	3-point bending	Web in tension	835	750	49.96	100.97	3.94	3.85
C 100×50×4×4-4-u	4-point bending	Web in tension	835	750	49.99	100.28	3.97	3.96
C 100×50×6×9-3-n	3-point bending	Web in compression	849	750	49.47	100.38	8.73	5.98
C 100×50×6×9-4-n	4-point bending	Web in compression	847	750	49.52	100.3	8.83	6.01
C 100×50×6×9-3-u	3-point bending	Web in tension	849	750	49.51	100.35	8.84	5.96
C 100×50×6×9-4-u	4-point bending	Web in tension	848	750	49.45	100.35	8.82	5.93

Table 3: Material properties from tensile coupon tests

Specimen	t (mm)	E (N/mm^2)	f_y (N/mm^2)	$f_{1.0}$ (N/mm^2)	f_u (N/mm^2)	ε_u (%)	ε_f (%)	R-O parameters	
								n	$n_{0.2,1.0}$
A 50×50×4	3.93	190400	299	387	600	50	62	4.1	3.6
A 100×65×11	10.78	189100	290	342	621	51	63	5.5	2.2
C 40×40×5×5	4.96	190200	292	383	659	57	69	4.8	3.5
C 100×50×4×4	3.92	190100	289	384	687	60	69	4.1	3.3
C 100×50×6×9 W	6.00	184800	258	340	576	49	64	3.7	3.3
C 100×50×6×9 F	8.95	195700	275	337	604	51	67	5.8	2.5

Table 4: Material properties from mill certificates

Specimen	Grade	$f_{y,mill}$ (N/mm^2)	$f_{1.0,mill}$ (N/mm^2)	$f_{u,mill}$ (N/mm^2)	$\varepsilon_{f,mill}$ (%)
A 50×50×4	EN 1.4571	274	311	575	54
A 100×65×11	EN 1.4307	348	382	634	53
C 40×40×5×5	EN 1.4307	305	353	638	54
C 100×50×4×4	EN 1.4307	287	322	631	57
C 100×50×6×9 W	EN 1.4404	295	346	586	53
C 100×50×6×9 F	EN 1.4404	277	313	576	54

Table 5: Measured initial geometric imperfections

Specimen	w_{fl1} (mm)	w_{fl2} (mm)	w_{web} (mm)	w_0 (mm)
A 50×50×4	0.14	0.10	-	0.14
A 100×65×11	0.39	0.12	-	0.39
C 40×40×5×5	0.48	0.29	0.30	0.48
C 100×50×4×4	0.51	0.72	0.36	0.72
C 100×50×6×9	0.38	0.21	0.13	0.38

Table 6: Key results from angle tests

Specimen	Outstand flange (compression)		Outstand web (bending)		M_u (kNm)	M_u/M_{el}	M_u/M_{pl}	M_u/M_{EC3}	R_m	R_u
	c/tε	Class	c/tε	Class						
A 50×50×4-3	14.5	4	14.3	1	4.10	2.51	1.40	2.56	4.3	>9.0
A 50×50×4-4	14.4	4	14.3	1	3.45	2.11	1.17	2.16	32.7	>52.9
A 100×65×11-3	7.1	1	10.9	1	34.89	2.42	1.36	1.36	12.8	>12.8
A 100×65×11-4	7.2	1	11.0	1	28.23	1.96	1.10	1.10	16.4	>16.4

Table 7: Key results from channel tests

Specimen	Internal web (compression)		Outstand flange (bending)		M_u (kNm)	M_u/M_{el}	M_u/M_{pl}	M_u/M_{EC3}	R_m	R_u
	c/tε	Class	c/tε	Class						
C 40×40×5×5-3-n	7.6	1	8.6	1	3.50	3.54	2.06	2.06	21.2	>25.9
C 40×40×5×5-4-n	7.8	1	8.4	1	2.87	2.81	1.64	1.64	26.5	>38.3
C 40×40×5×5-3-u	-*	-*	8.7	1	3.19	3.22	1.87	1.87	7.2	>10.3
C 40×40×5×5-4-u	-*	-*	8.5	1	2.95	2.98	1.73	1.73	22.3	>22.3
C 100×50×4×4-3-n	26.9	3	13.6	1	4.59	3.11	1.73	3.11	16.5	>25.0
C 100×50×4×4-4-n	27.9	3	13.7	1	3.78	2.56	1.42	2.56	48.3	>48.3
C 100×50×4×4-3-u	-*	-*	13.6	3	3.61	2.46	1.36	2.46	3.5	4.6
C 100×50×4×4-4-u	-*	-*	13.5	3	3.08	2.09	1.16	2.09	4.4	6.6
C 100×50×6×9-3-n	15.5	1	5.6	1	8.36	3.04	1.69	1.69	18.7	>18.7
C 100×50×6×9-4-n	15.4	1	5.5	1	7.37	2.73	1.52	1.52	50.0	>68.7
C 100×50×6×9-3-u	-*	-*	5.5	1	9.23	3.35	1.87	1.87	17.1	>17.1
C 100×50×6×9-4-u	-*	-*	5.5	1	7.48	2.77	1.54	1.54	21.4	>26.2

Note: * Internal web element is in tension in the 'u' configuration

Table 8: Effect of moment gradient

Specimen	Class	$M_{u,3}/M_{u,4}$	$R_{m,3}/R_{m,4}$	$R_{u,3}/R_{u,4}$
A 50×50×4	4	1.19	0.13	0.17
A 100×65×11	1	1.24	0.78	0.78
C 40×40×5×5-n	1	1.22	0.80	0.68
C 40×40×5×5-u	1	1.08	0.32	0.46
C 100×50×4×4-n	3	1.22	0.34	0.52
C 100×50×4×4-u	3	1.17	0.80	0.70
C 100×50×6×9-n	1	1.13	0.37	0.27
C 100×50×6×9-u	1	1.24	0.80	0.65
MEAN		1.19	0.54	0.53
COV		0.04	0.48	0.38

Table 9: Location of ENA, PNA and distance between the two.

Specimen	y_{el} (mm)	y_{pl} (mm)	y_{el}-y_{pl} (mm)	$(y_{el}-y_{pl})/h$
A 50×50×4	14.16	3.99	10.17	0.20
A 100×65×11	34.09	22.61	11.48	0.11
C 40×40×5×5	15.57	13.17	2.40	0.06
C 100×50×4×4	14.11	3.75	10.36	0.21
C 100×50×6×9	16.88	10.70	6.18	0.12